

# We are IntechOpen, the world's leading publisher of Open Access books Built by scientists, for scientists

6,900

Open access books available

185,000

International authors and editors

200M

Downloads

Our authors are among the

154

Countries delivered to

TOP 1%

most cited scientists

12.2%

Contributors from top 500 universities



WEB OF SCIENCE™

Selection of our books indexed in the Book Citation Index  
in Web of Science™ Core Collection (BKCI)

Interested in publishing with us?  
Contact [book.department@intechopen.com](mailto:book.department@intechopen.com)

Numbers displayed above are based on latest data collected.  
For more information visit [www.intechopen.com](http://www.intechopen.com)



---

# Nuclear Pollution in the East China Sea from the Fukushima Disaster

---

X. San Liang and Yineng Rong

Additional information is available at the end of the chapter

<http://dx.doi.org/10.5772/intechopen.80016>

---

## Abstract

Nuclear pollution has become a new form and perhaps more harmful type of pollution that obsesses coastal regions; it has been of increasing concern after the disastrous Fukushima nuclear leak on March 11, 2011. In order to assess the impact of the Fukushima accident on the East China Sea (ECS), a highly resolved model is set up to simulate the evolution of the  $^{137}\text{Cs}$  concentration. Different from previous studies in this regard, here we take into account the radionuclides originally existing in the ocean. It is found that the radionuclides from the Fukushima leak do have reached ECS, though with a concentration far below the harmful level. The major waterways that inlet the radionuclides are Taiwan Strait and the waterway east of Taiwan. The radioactive material tends to accumulate in the ECS until reaching its peak in 2019; afterward, the outflux through Tokara Strait and Tsushima exceeds the influx through the two southern waterways, and the material resumes in 2021 to its original state. The concentration is neither homogeneously nor stationarily distributed; for example, usually in summer, there is a high center over the Subei Bank in the Yellow Sea. This study is expected, should a similar accident happen again, to help decide where to monitor the ocean, and, hopefully, how to get the pollution under control.

**Keywords:** Yellow Sea, East China Sea, Fukushima nuclear leak, nested ocean modeling

---

## 1. Introduction

The coastal seas are the most severely polluted waters in the world ocean. As shown in the preceding chapter, runoff from urban areas and agricultural fields, plus the deposition from

the atmosphere, may lead to harmful algal bloom and the formation of dead zone due to hypoxia and eutrophication. In recent years, a new type of coastal pollution has been of great concern, that is, the nuclear pollution due to nuclear power plant failure.

Historically, the most disastrous catastrophic nuclear disaster, in terms of cost and casualty, is the Chernobyl accident. The disaster began on April 26, 1986, with a late-night safety test at the fourth light water graphite moderated reactor at the Chernobyl Nuclear Power Plant, Ukrainian Soviet Socialist Republic of the former Soviet Union, which, however, ended with a destructive steam explosion that lofted plumes of fission products into the atmosphere (emission of radionuclides totals up to  $13,000 \times 10^{15}$  Bq; [1]), exerting a widespread influence on Europe, Asia, and America [2]. Second to it is the nuclear energy disaster at Fukushima Daiichi Nuclear Power Plant, 150 miles northeast of Tokyo, Japan, which is also of the maximum classification (classified as a level 7 event on the International Nuclear Event Scale). An earthquake of magnitude 9.0 (Tōhoku earthquake) on March 11, 2011, caused a devastating tsunami with a wave reaching as high as 16 meters, overwhelming the Fukushima I Nuclear Power Plant's seawall (10 m high). The cooling systems of the plant were knocked out, and the insufficient cooling resulted in a series of nuclear meltdowns, hydrogen-air chemical explosions, and the release of radioactive material into the ambient environment [3].

The impact of the Fukushima accident can never be overestimated; it has been ranked as the world's worst nuclear accident in 25 years. The radionuclides have been widely spread with the winds and oceanic circulations; particularly, it is reported that they arrive above North America just 4 days after [4]. Although the emission is claimed to have been under control, the impact, particularly the impact on the oceans, remains [5, 6]. For example, the concentration of  $^{137}\text{Cs}$  off Japan, though has been on decline ever since the accident, remains as high as 100 times that before the accident by October 2014 [7]. By simulation, the radionuclides may reach the US coast in 4–5 years [8, 9] and then come back along the equator, impacting the coastal oceans in Southeast Asia. In this chapter, we focus on its impact on the East China coast, one of the most densely populated regions in the world. Since  $^{137}\text{Cs}$  has the longest life cycle (with a half-life period  $\tau = 30$  year), in the following, only  $^{137}\text{Cs}$  is considered.

Previously, the East China coast is believed to be not or less influenced by the accident [10]. Research during the past few years, however, shows that the Fukushima-originated  $^{137}\text{Cs}$  has already arrived in the China Seas. By Zhao et al. [11] and Rong et al. [12], it arrives in 2013 and will continue to accumulate in the following 5–6 years. Considering that the previous modeling studies do not take into account the background  $^{137}\text{Cs}$  distributions, and may generally have too coarse a resolution for the East China Sea, recently Rong and Liang [13] reexamine the problem with a highly resolved numerical model, plus a sequential updating strategy to assimilate the background  $^{137}\text{Cs}$  concentration, and reveal how the intruded radionuclide may move, evolve, reside, or disappear. This chapter is a summary of these results. The following is mainly based on Rong et al. [12] and Rong and Liang [13], where Sections 2 and 3 give a brief introduction of the model configuration and simulation strategy, Section 4 is a validation, Section 5 shows the results, and Section 6 concludes the study.

## 2. Model setup

In Rong and Liang [13], the Regional Ocean Modeling System (ROMS) is adopted for the simulation and prediction of the radionuclide transport. ROMS is a widely applied incompressible ocean model with free surface, hydrostatic, and Boussinesq approximations; it uses the Reynolds average Navier-Stokes equations as governing equations (e.g., [14]). In Cartesian coordinates  $(x, y, z)$ , these equations are:

$$\frac{\partial u}{\partial t} + \vec{v} \cdot \nabla u - fv = -\frac{1}{\rho_0} \frac{\partial P}{\partial x} - \frac{\partial}{\partial z} \left( \overline{u'w'} - \gamma \frac{\partial u}{\partial z} \right) + F_u + D_u \quad (1)$$

$$\frac{\partial v}{\partial t} + \vec{v} \cdot \nabla v - fu = -\frac{1}{\rho_0} \frac{\partial P}{\partial y} - \frac{\partial}{\partial z} \left( \overline{v'w'} - \gamma \frac{\partial v}{\partial z} \right) + F_v + D_v \quad (2)$$

$$\frac{\partial P}{\partial z} = -\rho g \quad (3)$$

$$\frac{\partial u}{\partial x} + \frac{\partial v}{\partial y} + \frac{\partial w}{\partial z} = 0 \quad (4)$$

$$\frac{\partial C}{\partial t} + \vec{v} \cdot \nabla C = -\frac{\partial}{\partial z} \left( \overline{C'w'} - \gamma_\theta \frac{\partial C}{\partial z} \right) + F_C + D_C \quad (5)$$

where  $\vec{v} = (u, v, w)$  is the three-dimensional velocity vector,  $C$  is the concentration of some tracer,  $F$  denotes external forcing,  $D$  represents the horizontal dissipation/diffusion processes, and the other symbols are conventional. This equation set is closed with an equation of state:

$$\rho = \rho(T, S, P) \quad (6)$$

and parameterized turbulent fluxes; particularly, the vertical mixing is parameterized with a nonlocal, K-profile parameterization (KPP) scheme [15]. The closed set of equations are transformed into terrain-following coordinates  $(x, y, \sigma)$  and then solved using a split-explicit scheme.

A one-way nesting strategy is used, and hence two model domains are considered (**Figure 1**). The outer domain (L0) comprises the whole North Pacific Ocean, from the equator to Bering Strait. The inner domain (L1) covers the East China Sea (ECS) region. For both domains, there are 22 sigma levels in the vertical, while horizontally the resolutions for L0 and L1 are roughly 10.1 and 3.6 km, respectively. Other parameters are referred to **Table 1**. The bottom topography is extracted from the ETOPO1 data by National Oceanic and Atmosphere Administration (NOAA). A Hanning filter is applied to the topography to make sure that pressure gradient force is computed accurately [16].

The horizontal boundaries for model L0 are all taken as closed. This makes sense because (1) Bering Strait is very narrow and shallow and (2) the equator is a dynamically closed boundary, though in reality there does exist cross-equator water exchange. This makes the long-time integration much reliable. For model L1, the boundary fluxes are supplied by the outputs from

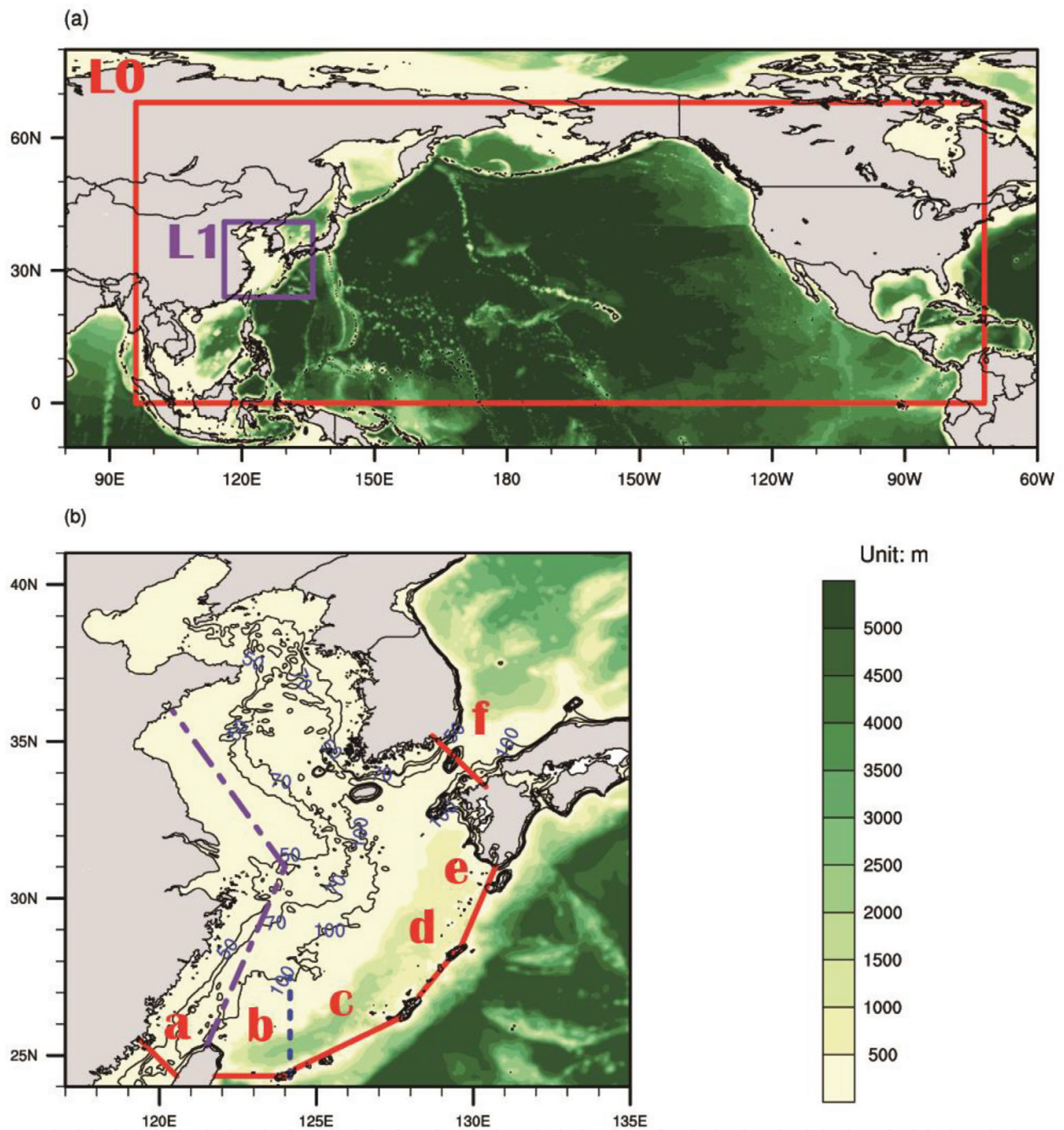


**Figure 1.** Bathymetry (in m) for the two-domain, one-way nesting model. Shown are the positions where the fluxes are calculated: a. Taiwan Strait, b. East of Taiwan, c. Ishigaki to Naha, d. Naha to Amami, e. Tokara Strait, f. Tsushima Strait. Also marked is a section of East China coast (green line).

| Domain | Maximum depth (m) | Minimum depth (m) | Latitude (°N) | Longitude (°E) | Resolution (km) | Time step (s) |
|--------|-------------------|-------------------|---------------|----------------|-----------------|---------------|
| L0     | 5000              | 15                | 0–68          | 96–288         | 10.1            | 900           |
| L1     | 5000              | 10                | 24–41         | 117–135        | 3.6             | 90            |

**Table 1.** Parameters for the two-domain nested ROMS model.

coarse model. The nesting is realized through the pointer-based ROMS2ROMS Matlab (Agrif) package [17]. To this model, tides are applied; specifically, the 10 tidal constituents, M2, S2, N2, K2, K1, O1, P1, Q1, Mf, and Mm, are considered here (data from Oregon State University; see [18, 19]). In the vertical direction, the no-flux condition is applied at the bottom. At the surface, wind stress, heat, and freshwater fluxes are prescribed. The stress and fluxes are from two datasets. Between January 2001 and August 2015, they are from the reanalysis data of National Centers for Environmental Prediction (NCEP, daily,  $2.5^\circ$  (lat)  $\times$   $2.5^\circ$  (lon)). After August 2015, the predicted data of Geophysical Fluid Dynamics Laboratory (GFDL, 3 hour,  $2^\circ$  (lat)  $\times$   $2.5^\circ$  (lon)) are used.

The model is initialized with the fields of temperature, salinity, velocity, and sea surface height derived from the HYbrid Coordinate Ocean Model (HYCOM,  $1/12^\circ$ ) reanalysis dataset. The  $^{137}\text{Cs}$  concentration is prescribed at two steps. (1) Initially, it is estimated using the data from International Atomic Energy Agency (IAEA, <https://maris.iaea.org/Search/Search.aspx>) with a simple assimilation scheme (see below). (2) Upon occurrence of the accident, the released  $^{137}\text{Cs}$  is poured into the ocean. Here arise the following issues: how much is the pollutant; when and where to introduce the pollutant. Note that the total amount of the leaked  $^{137}\text{Cs}$  remains largely unknown. It has been estimated that the release into the atmosphere of  $^{137}\text{Cs}$  is in the range of 13–15 PBq (1 PBq =  $10^{15}\text{Bq}$ ; Chino et al., 2011) and that poured directly into the ocean is 2.3–27 PBq [20–22]; we will choose 5 PBq in the standard run and do some experiments with the amount in this range. Second, the release of the  $^{137}\text{Cs}$  is actually continuous at one grid point during March–April 2011 [5, 20, 23]. But since it has been found [24] that, for a long-time simulation, no significant difference shows for different release strategies, it is assumed that the leak is instantaneous on April 1, 2011. Besides, to avoid shock, the radionuclide is homogeneously distributed within an area centered at the leak location ( $37.42^\circ\text{N}$ ,  $141.03^\circ\text{E}$ ) with a radius of  $2^\circ$ ; vertically, it has a profile gradually decreasing linearly from the surface to 0 at 100 m deep.

### 3. Assimilation of the background $^{137}\text{Cs}$ concentration

During 1950–1990, plenty of radioactive substances had been poured into the oceans until the Chernobyl accident occurred and the Comprehensive Nuclear-Test-Ban Treaty was signed; it is believed that, by 1986, the  $^{137}\text{Cs}$  in the oceans has totaled 800 PBq [25]. Considering that the release in this accident is no more than 42 PBq [21], the major part of the  $^{137}\text{Cs}$  in the Pacific cannot be from Fukushima. This is particularly true for regions far away from the Plant. As an evidence, the IAEA data show that the average  $^{137}\text{Cs}$  concentration in the surface layer (0.5 m) of the North Pacific is  $1.54\text{ Bq/m}^3$  during the decade before the accident, while previous studies neglecting the contribution from the background concentration (e.g., [9, 11, 23, 26]) reveal a maximum after-accident concentration less than  $0.5\text{ Bq/m}^3$  in ECS, which is, obviously, far below the observation.

The  $^{137}\text{Cs}$  distribution before the accident thence must be taken into account. In this study, two different simulations are performed. Run 1 as a control run does not have the background concentration; 5PBq of  $^{137}\text{Cs}$  is directly poured into the ocean at the accident time just as

Hideyuki et al. [27] and Zhao et al. [11]. Run 1 runs from April 1, 2011 to March 31, 2021. Assume that the regions where the  $^{137}\text{Cs}$  concentration in Run 1 is less than  $0.001 \text{ Bq/m}^3$  are not affected by the pollutant directly poured into the Pacific. The observational data in these regions from January 2001 to February 2011 are then used as the observed  $^{137}\text{Cs}$  concentration. These data are assimilated into the model to form an optimal estimate of the field, which is taken as the background concentration for the next run, i.e., Run 2.

The assimilation is through a scheme called sequential updating which, albeit simple, has been successfully utilized in the many operational ocean forecasts, such as in the forecast of the Iceland-Faeroe frontal variability [28, 31]. It is made up of two steps. First, use objective analysis (OA) to prepare the observational field for assimilation. The e-folding time and distance for OA are, respectively, 360 days and  $40^\circ$ . An error field is obtained accordingly. Second, an optimal interpolation (OI) is performed to combine the model output and the OAd field, with the inverse of the error field as the weight. The OI may be performed globally or pointwise. The two do not seem to make much difference; for ease to implement, the latter is hence adopted. In this way, the model output is sequentially updated with the observation.

**Table 2** lists the observed surface (0.5 m)  $^{137}\text{Cs}$  concentrations in the China Seas before the accident [29] and our corresponding results. For all the six available observations, the mean relative error is 10.3%. Compared to the zero distribution in previous studies, our model works well to produce the  $^{137}\text{Cs}$  distribution before the accident.

Since only the surface observation is available, the vertical  $^{137}\text{Cs}$  distribution has to be empirically set. We follow Tsumune et al. [30] to set:

$$C(z) = C_0 \times 10^{-0.0005z}, \quad (7)$$

where  $C$  (in  $\text{Bq/m}^3$ ) indicates the  $^{137}\text{Cs}$  concentration; particularly,  $C_0$  is the surface concentration. This, together with the measurements/estimates of the  $^{137}\text{Cs}$  concentration immediately after the accident, furnishes the initial condition for Run 2, which is used for the simulation and prediction.

| Latitude | Longitude | Observations ( $\text{Bq/m}^3$ ) | Simulation results                |                     |
|----------|-----------|----------------------------------|-----------------------------------|---------------------|
|          |           |                                  | Concentration ( $\text{Bq/m}^3$ ) | Relative errors (%) |
| 32.01    | 126.48    | $1.01 \pm 0.06$                  | 1.22                              | 20                  |
| 36.05    | 123.50    | $1.10 \pm 0.07$                  | 1.20                              | 10                  |
| 20.50    | 122.29    | $1.14 \pm 0.07$                  | 1.25                              | 9                   |
| 29.64    | 123.04    | $1.32 \pm 0.13$                  | 1.19                              | -10                 |
| 32.00    | 124.00    | $1.33 \pm 0.10$                  | 1.19                              | -11                 |
| 18.00    | 116.00    | $1.42 \pm 0.09$                  | 1.38                              | -2                  |

**Table 2.** Comparison of surface layer (0.5 m)  $^{137}\text{Cs}$  radioactive concentration between the observations [29] and simulations in this study.

## 4. Validation

### 4.1. Outer domain: SST and currents

Our simulated result has been compared with the data derived from the Simple Ocean Data Assimilation (SODA). **Figure 2** shows the 2009 annual mean sea surface temperature (SST) and flow from our simulation (**Figure 2a**) and SODA (**Figure 2b**). It is easily seen that the major features of the SST have been well reproduced. For example, shown in the figure are the east-west asymmetry of the temperature in the tropic and the warm pool in the western equatorial Pacific. The large-scale circulations have also been well reproduced. The North Equatorial Current flows westward, encounters the west boundary, and forms the Kuroshio and the much more energetic current, the Ryukyu Current. Upon passing the Luzon, part of the Kuroshio may intrude into the northern South China Sea (SCS) in an anticyclonic form, but the mainstream keeps moving northward into the ECS. The Kuroshio in ECS branches to the northeast of Taiwan. One branch intrudes onto the shelf, forming the outer part of the Taiwan Warm Current and then merging back into the mainstream at a higher latitude. The Kuroshio flows out of the ECS through Tokara Strait, meeting the Oyashio Current off the Japan coast near Fukushima. It then flows eastward, in a meandering form, and makes the Kuroshio Extension System. These currents are evident in both **Figure 2a** and **b**, and they in these two subfigures are similar in magnitude and location. Our simulation of the large-scale system is therefore successful.

### 4.2. East China Sea: SST and currents

The comparison of the ECS circulation and SST is with the HYCOM product. **Figure 3** shows the monthly mean (2006–2011) ECS SST and velocity. The left and right panels are, respectively, the simulated result and the HYCOM data. Note that East Asia has a monsoon climate; correspondingly, the ocean fields have strong seasonal variations. By comparing the SST and flow season by season, clearly the two panels agree well in both summer and winter, except in

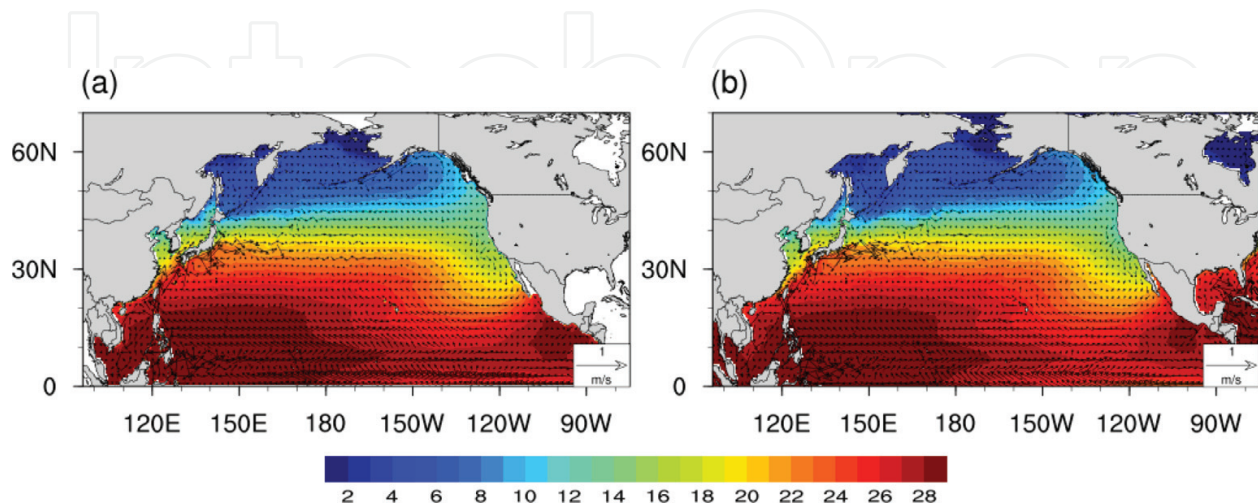


**Figure 2.** Annual mean SST (shaded) and surface velocity (vector) of 2009 in North Pacific: (a) model output, (b) SODA data.

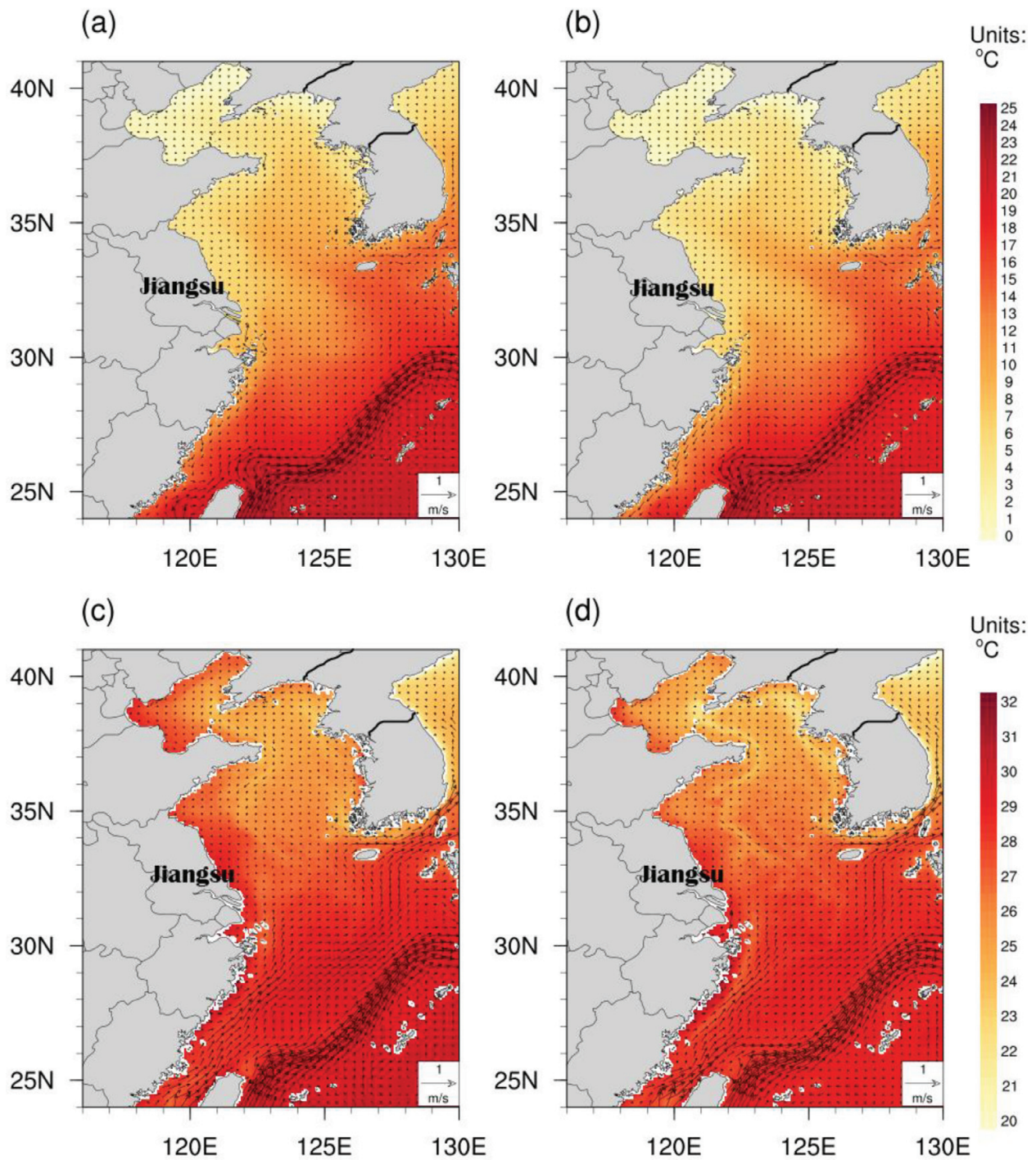


**Figure 3.** The ECS SST (shaded) and velocity (vector) in winter and summer: (a) ROMS outputs, February; (b) HYCOM result, February; (c) ROMS outputs, August; (d) HYCOM result, August.

August when HYCOM displays a higher SST at the mouth of the Bohai Sea. The general features of the ECS circulation system have all been captured. For example, in winter (February), the coastal SST is lower than the open sea. West of Cheju Island, a warm tongue intrudes northwestward into the waters south of Shandong Peninsula. At this time, the Kuroshio, the Taiwan Warm Current, and the Tsushima Current are weak, and the Zhe-Min Coastal Current

is southward. In summer (August, **Figure 3c and d**), the Kuroshio and its branch are strong, and the Zhe-Min Coastal Current flows northward. Scattered in the Yellow Sea are isolated cold patches; they are especially clear off the tips of Shandon Peninsula. These features are well known and have been successfully reproduced here. This completes the validation.

#### 4.3. A comparison of the $^{137}\text{Cs}$ distribution simulations with and without background concentration assimilation

**Table 3** shows the differences between simulations with (Run 2) and without (Run 1) assimilating the  $^{137}\text{Cs}$  background radioactive concentration in the North Pacific. Clearly, in Run 1, there are many regions where  $^{137}\text{Cs}$  has been observed, but the simulated concentration is zero. This simulation has been greatly improved in Run 2, where the concentrations at these

| Date       | Latitude (°N) | Longitude (°E) | Observation (Bq/m <sup>3</sup> ) | Run 1 (Bq/m <sup>3</sup> ) | Run 2 (Bq/m <sup>3</sup> ) |
|------------|---------------|----------------|----------------------------------|----------------------------|----------------------------|
| 3/01/2012  | 22.11         | 191.46         | 1.6                              | 0                          | 1.49                       |
| 05/01/2012 | 22.97         | 179.98         | 1.6                              | 0                          | 1.48                       |
| 21/01/2012 | 34.45         | 130.08         | 1.7                              | 0                          | 1.22                       |
| 21/01/2012 | 34.45         | 130.08         | 1.4                              | 0                          | 1.22                       |
| 22/01/2012 | 32.53         | 132.98         | 1.6                              | 0                          | 1.34                       |
| 22/01/2012 | 32.53         | 132.98         | 1.3                              | 0                          | 1.34                       |
| 29/01/2012 | 26.89         | 182.06         | 1.6                              | 0.01                       | 1.75                       |
| 30/01/2012 | 27.84         | 189.1          | 2.1                              | 0                          | 1.76                       |
| 31/01/2012 | 32.98         | 197.06         | 1.7                              | 4.08                       | 2.55                       |
| 01/02/2012 | 33.05         | 204.72         | 1.6                              | 0                          | 3.01                       |
| 02/02/2012 | 34.26         | 213.1          | 2                                | 0                          | 1.69                       |
| 03/02/2012 | 35.16         | 220.91         | 2.2                              | 0                          | 1.7                        |
| 04/02/2012 | 48.99         | 219.18         | 1.3                              | 0                          | 1.41                       |
| 04/02/2012 | 36.36         | 228.83         | 1.7                              | 0                          | 1.66                       |
| 05/02/2012 | 47.53         | 228.13         | 1.4                              | 0                          | 1.41                       |
| 17/02/2012 | 26.82         | 173.34         | 2.4                              | 0.12                       | 1.6                        |
| 24/02/2012 | 32.29         | 206.67         | 1.6                              | 0                          | 4.08                       |
| 29/02/2012 | 34.53         | 175.9          | 9.6                              | 1.81                       | 5.72                       |
| 02/03/2012 | 33.42         | 196.11         | 2.1                              | 1.61                       | 2.18                       |
| 02/03/2012 | 39.46         | 177.47         | 13.6                             | 4.53                       | 12.38                      |
| 04/03/2012 | 30.09         | 211.27         | 1.7                              | 0                          | 1.58                       |
| 09/03/2012 | 40.45         | 133.84         | 1.7                              | 0                          | 1.11                       |
| 16/03/2012 | 31.92         | 223.18         | 1.6                              | 0                          | 1.71                       |
| 21/03/2012 | 34.86         | 177.27         | 5.8                              | 3.77                       | 2.34                       |

**Table 3.**  $^{137}\text{Cs}$  concentrations from the IAEA observations, Run 1 and Run 2 (January–March, 2012).

locations are now close to the observations. As another issue, concentration may vary dramatically in 1 day (such as January 21, 2012, in **Table 3**). By comparing the observations from IAEA (124 different stations from June, 2011, to September, 2012, throughout the North Pacific) with the two Runs, it is found that the average relative deviation of the Run 1 simulations from the observations is 103.06%. In contrast, that of the Run 2 simulations is only 27.58%. If one recalls that the average relative interdiurnal variation of the observations is as high as 20.69%, the success of Run 2 is really remarkable. That is to say, the  $^{137}\text{Cs}$  simulation has been greatly improved with the background concentration assimilated.

## 5. Impact on the East China coast

### 5.1. $^{137}\text{Cs}$ flux

The ECS is a half-closed marginal sea in the Northwest Pacific, connected to the open ocean through several narrow waterways, which include Taiwan Strait, Tokara Strait, Tsushima Strait, and the channels between Taiwan and Yonaguni, Ishigaki and Naha, and Naha and Amami. To see how the Fukushima nuclear substances may intrude into ECS, the  $^{137}\text{Cs}$  fluxes across these six waterways are computed. From **Figure 4**, Taiwan Strait (**Figure 4a**) and the Taiwan-Yonaguni channel (**Figure 4b**) are the major straits that introduce the pollutants. The influx of  $^{137}\text{Cs}$  East of Taiwan is, on average,  $3.99 \times 10^7 \text{Bq/s}$ , which is an order larger than that through Taiwan Strait ( $3.82 \times 10^6 \text{Bq/s}$ ). However, considering that the Kuroshio Branch Current makes only a small fraction of Kuroshio, its impacts on the China coastal regions could be of the same order. Generally, these fluxes show significant temporal variabilities. For the flux through Taiwan Strait, seasonality is obvious, with a high concentration in summer and a low concentration in winter. Meanwhile, there also exists a clear interannual variability: the flux is increasing during 2014–2017 and decreasing otherwise. For the strait east of Taiwan, the variability is mostly interannual. Before 2013, the flux grows rapidly. It finds its second growth in early 2014, reaching its peak in 2017. After that, it declines gradually.

The other waterways near Taiwan include the section from Ishigaki to Naha (**Figure 4c**) and that from Naha to Amami Islands (**Figure 4d**). These sections are roughly parallel to the Kuroshio axis. With a water depth of 1500 m or so, they are also the main straits that connect ECS with Northwest Pacific. From the figure, it is seen that large amount of  $^{137}\text{Cs}$  is transported between Northwest Pacific and ECS. But because of the alignment, which is parallel to the Kuroshio path, the average fluxes in both waterways are orders smaller (respectively,  $4.44 \times 10^5 \text{Bq/s}$  and  $5.79 \times 10^5 \text{Bq/s}$ ) than those east of Taiwan and through Tokara Strait (see below).

Tokara Strait (**Figure 4e**) and Tsushima Strait (**Figure 4f**) are the two waterways that outlet the ECS radionuclides. The flux through the latter is  $2.58 \times 10^6 \text{Bq/s}$ , while that through the former is an order larger, reaching  $4.26 \times 10^7 \text{Bq/s}$ . It is interesting to note that the fluxes east of Taiwan and that through Tokara Strait are similar in magnitude and in variation pattern. This implies that most of the  $^{137}\text{Cs}$  into ECS along the Kuroshio actually does not stay within the

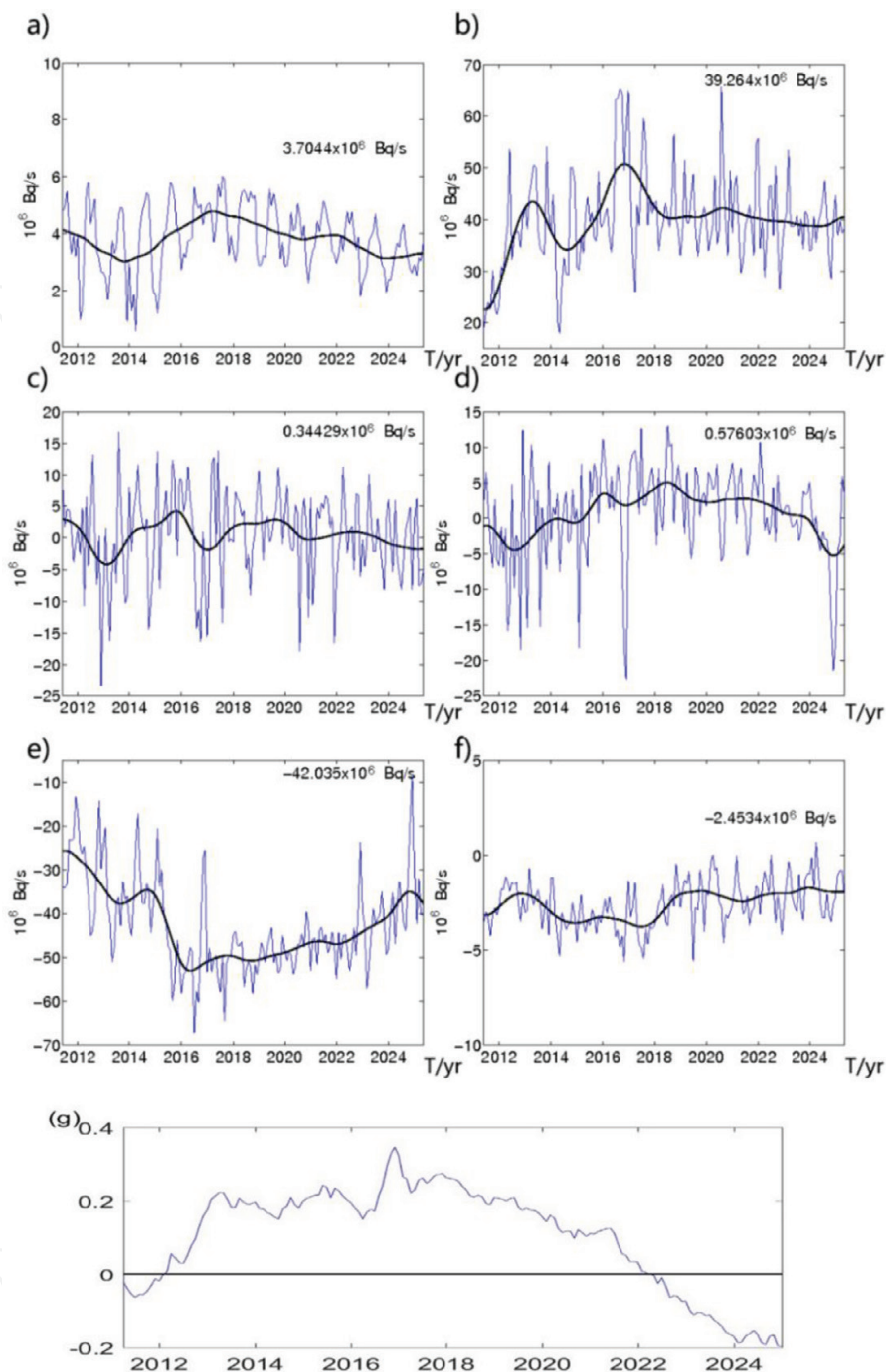


**Figure 4.** Time series of the  $^{137}\text{Cs}$  fluxes across the six waterways indicated in **Figure 1b** (a–f; unit:  $\frac{10^6 \text{ Bq}}{\text{s}}$ ; positive values indicate fluxes into ECS; black lines are moving averages), and the total accumulation of nuclear pollutants in ECS (g; unit: PBq).

sea. Another feature is that the outfluxes through Tsushima Strait and Tokara Strait are weak in winter and strong in summer, in accordance with the seasonal variation of Kuroshio.

To see the net influx of the pollutant, we take a cumulative sum of the fluxes through the six waterways from April 2011 to December 2025. Shown in **Figure 4g** is the cumulant. Note the negative value before 2012. That means there is a net outflux of nuclear substance during that

period; in other words, the main part of  $^{137}\text{Cs}$  in the ocean has not arrived in ECS. After 2012, the nuclear substance begins to accumulate, though gradually, and reaches its peak in 2018 (0.13 PBq). In 2021, the sum is below zero again, implying that, in ECS, it takes about a decade for the radionuclide concentration to get back to its original level.

## 5.2. Nearshore distribution

Because of the dense population, we pay particular attention to the coastal regions. **Figure 5a** shows that the surface  $^{137}\text{Cs}$  concentration in ECS takes a maximum around 1.3–1.8 Bq/m<sup>3</sup>, depending on the location. Generally, it is high in the southeast of ECS and low in the northwest. The maximum is attained in 3 years after the accident along the Ryukyu Islands from Taiwan to

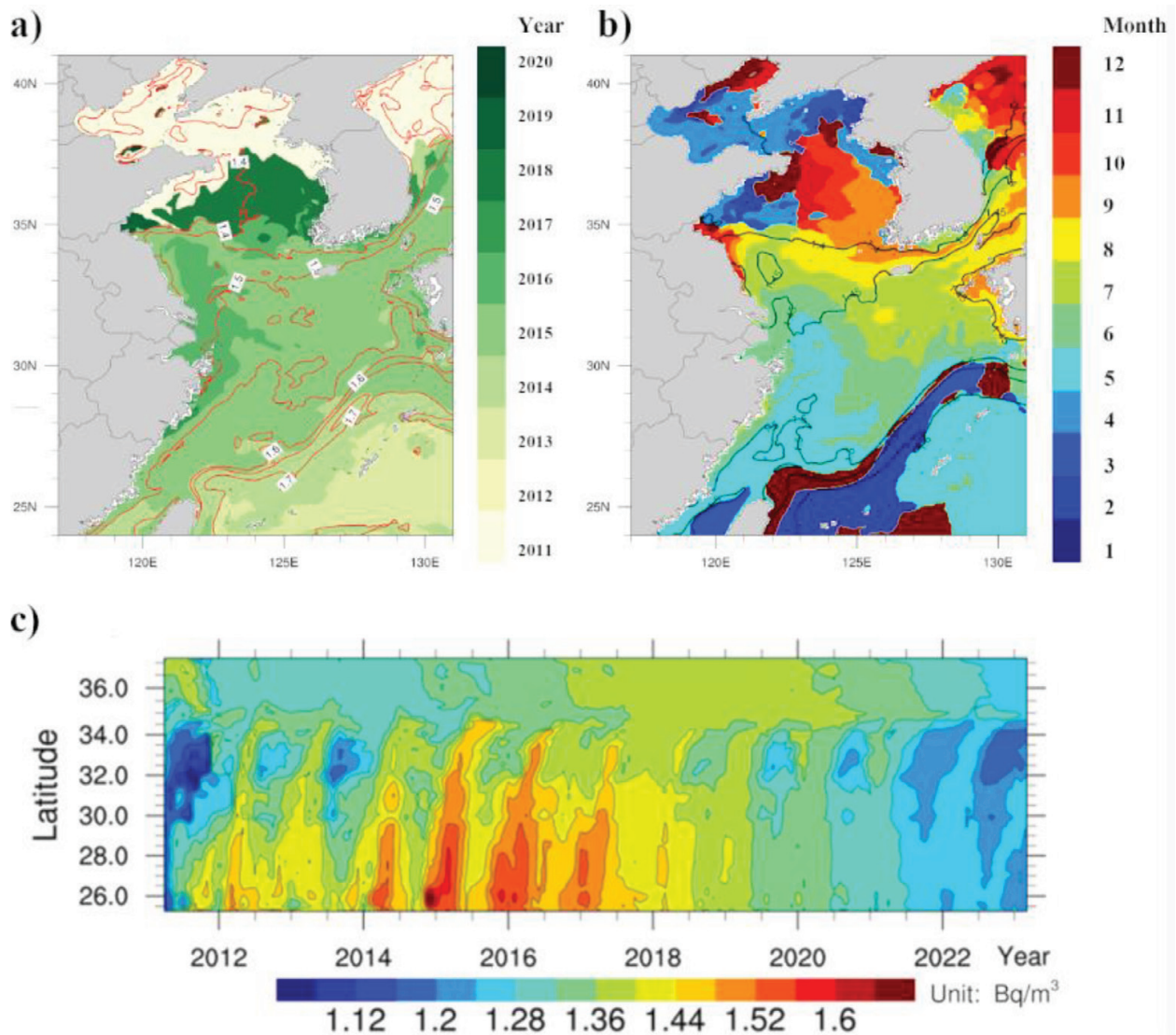


**Figure 5.** (a) Distribution of the simulated maximum surface  $^{137}\text{Cs}$  concentration (lines, in Bq/m<sup>3</sup>) and the year when it is attained (shaded). (b) Distribution of the maximal monthly mean  $^{137}\text{Cs}$  radioactive concentration (lines, in Bq/m<sup>3</sup>) and the months when the maximum is attained (shaded). The monthly mean is taken over the same months during 2014–2019. (c) Hovmöller diagram of the  $^{137}\text{Cs}$  concentration (shaded, in Bq/m<sup>3</sup>) between 25°N and 35°N (green line in **Figure 1b**) along the East China coast from 2011 to 2023.

Tokara Strait. On the whole, it peaks in 2014, except along the Zhejiang coast, where the peak appears 1 year later. In the Yellow Sea, the scenario looks much more complex. The maximal concentration is about 1.4–1.5 Bq/m<sup>3</sup>, but it varies with space and time. To the east of Harbor Lianyun, the maximum shows up in 2018; from Subei Shoal to Cheju Island, it appeared during 2014–2015; but from South Korea to Shandong Peninsula, it was attained in 2016. The concentrations in the Bohai Sea and Northern Yellow Sea and around the Shandong Peninsula remain at a level as that before the accident. That is to say, these regions are essentially not affected.

Based on the above, the East China coast is most severely affected during the period 2014–2018. A particular observation is that there exists a local high <sup>137</sup>Cs region (exceeding 1.45 Bq/m<sup>3</sup>) on the eastern side of the Subei Bank, a shallow water region off the middle Jiangsu coast.

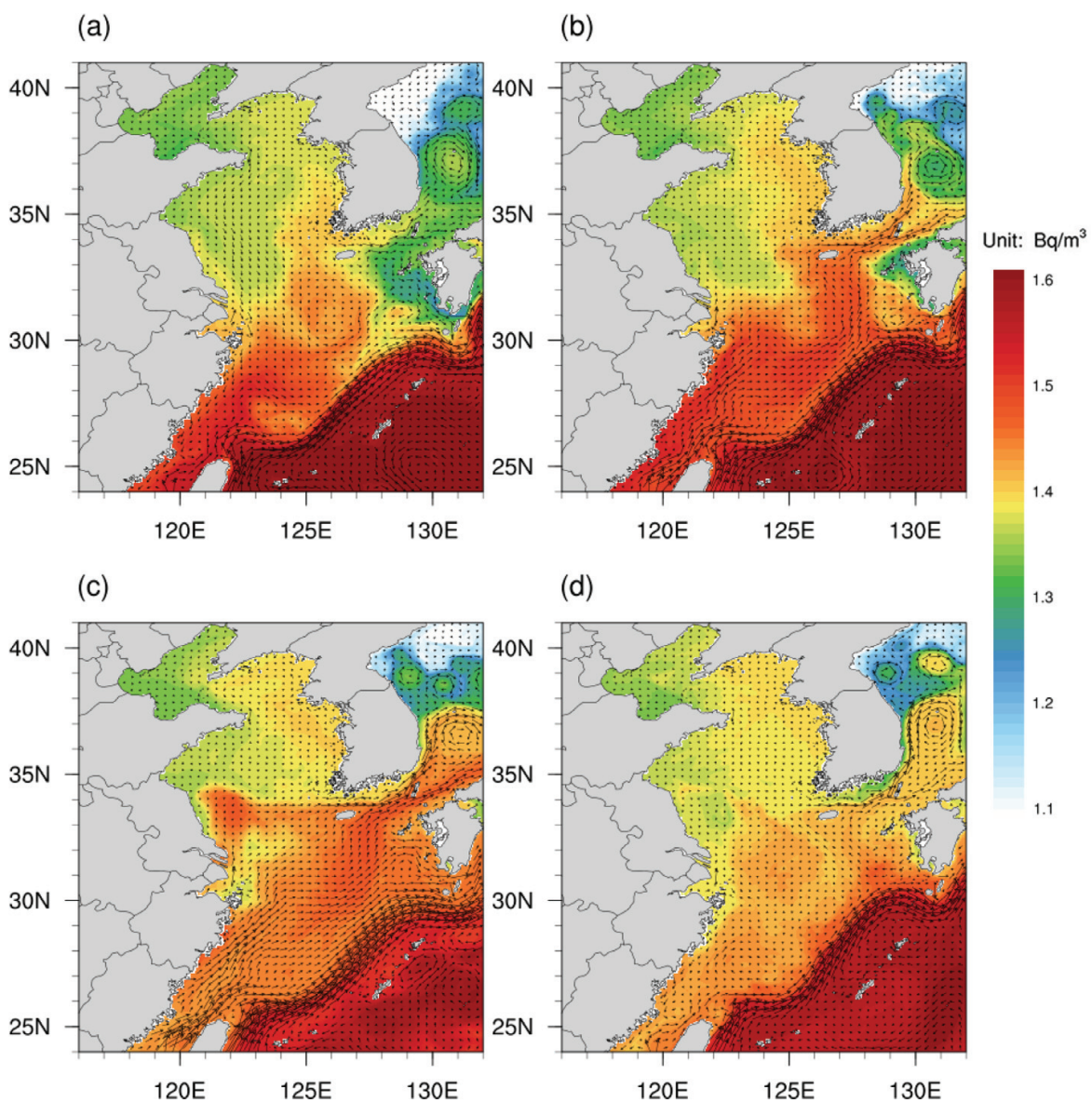


**Figure 6.** Distributions of the monthly mean surface <sup>137</sup>Cs concentration in ECS for (a) January, (b) April, (c) July, and (d) October of 2017.

**Figure 5c** is a Hovmöller diagram between 25°N and 35°N along the East China coast. From it, the maxima occur in the winter of every year before 2019 in the northern part of Taiwan Strait, spreading northward all the way to Subei Bank till summer.

In the Kuroshio region, the  $^{137}\text{Cs}$  concentration is high, and so is its horizontal gradient; that is to say, the strong current somehow functions to trap the radionuclide. Following the Kuroshio path to 35°N, one sees a concentration high in May-July. Along the Subei Coast, the maximum concentration is attained in August-November, while in the center of the Yellow Sea, the maximum takes place during September-November. For other regions such as the Bohai Sea and North Yellow Sea, the maximum appears in winter or early spring.

### 5.3. Seasonal variability

The above suggests that the surface  $^{137}\text{Cs}$  concentration in ECS varies considerably from season to season. To see more about this, **Figure 6** shows a sequence of the surface distribution in 2017. On the whole, the concentration displays a gradually decreasing trend northwestward, from roughly  $1.7 \text{ Bq/m}^3$  in the southeast to  $1.4 \text{ Bq/m}^3$  in the northwest. High-concentration water masses move mainly along the shelf break, following the Kuroshio path, from Taiwan toward Tokara Strait. That is to say, most of the nuclear substance influxing from east of Taiwan actually flows out of ECS; the major parts that affect the China coast are thence from within Taiwan Strait and through the Kuroshio Branch Current. In other words, they are with the Taiwan Warm Current (TWC), by which they are carried forth along the Zhe-Min Coast and Jiangsu Coast, and are finally transported out of ECS into the Sea of Japan through Tsushima Strait (**Figure 6d**). In the course, the remnants mostly stay along the Jiangsu Coast, leaving around the Subei Bank a high  $^{137}\text{Cs}$  concentration spot in summer (**Figure 6a** and **d**). We have also observed such a hotspot in other studies; see Chapter 2 for an example.

## 6. Concluding remarks

More than 6 years have passed since the Fukushima accident. The radionuclides from the disastrous nuclear leak have been identified in a lot of places in the world. Though there have been many studies, the impact of the accident on the local and global environment has not been well assessed. In this study, we find that the East China Sea (ECS), which was previously believed to be non- or less affected, actually has been full of the Fukushima pollutant, albeit the concentration is still far below a hazardous level.

Using a two-domain, one-way nesting ROMS model, we have simulated and predicted the  $^{137}\text{Cs}$  distribution and evolution in the ECS. The outer domain encloses the whole North Pacific which largely avoids the open boundary problem and hence allows for a reliable longer integration. The external forcings (winds, heat and freshwater fluxes, etc.) are either real (from available NCEP reanalysis data) or derived from the GFDL predictions. Different from the previous studies, this model takes into account the background concentration of the

radioactive  $^{137}\text{Cs}$  and has observations assimilated. The results have been carefully compared with the existing studies and observations and have been successfully validated.

By the simulation and prediction, the accumulated  $^{137}\text{Cs}$  in the ECS reaches its peak in 2018; after 10 years, it falls back to the level before the accident. The straits on both of Taiwan form the main waterways that inlet the radionuclide into ECS, and Tokara Strait and Tsushima Strait are the two through which they leave the region. It is found that the  $^{137}\text{Cs}$  concentration, especially that along the coast, varies from season to season. Usually, the pollution is most severe in winter; the maximal concentration along the East China coast reaches 1.3–1.8 Bq/m<sup>3</sup>. A conspicuous feature is the existence of a hotspot of high  $^{137}\text{Cs}$  concentration in summer around the Subei Bank, a shallow water region off Jiangsu, the most populous province of China. The times that the maxima are attained vary from 2014 to 2018, depending on the latitude. Generally, the higher the latitude, the later the maximum is attained.

We hope the above findings can help us to make policy for a rapid response to such kind of disasters. For example, should a more severe but similar leak happen again, we would first monitor the waterways on both sides of Taiwan, and the coastal regions such as the Subei Bank. Moreover, we can take actions in the waterways west and east of Taiwan in order to mitigate the situation and even get the pollution under control.

## Acknowledgements

We are grateful to IAEA for the  $^{137}\text{Cs}$  observations, to NGDC for the ETOPO1 data, to NOPP for the HYCOM data, and to NOAA for the SODA data, the reanalysis data, and the prediction data. This study was supported by the Jiangsu Provincial Government through 2015 Jiangsu Program for Innovation Research and Entrepreneurship Groups and through the Jiangsu Chair Professorship to XSL.

## Author details

X. San Liang\* and Yineng Rong

\*Address all correspondence to: [x.san.liang@gmail.com](mailto:x.san.liang@gmail.com)

School of Atmospheric Sciences and School of Marine Sciences, Nanjing University of Information Science and Technology, Nanjing, China

## References

- [1] Saenko V, Ivanov V, Tsyb A, Bogdanova T, Tronko M, Demidchik Y, et al. The Chernobyl accident and its consequences. *Clinical Oncology*. 2011;**23**(4):234-243. DOI: 10.1016/j.clon.2011.01.502

- [2] Povinec P, Chudý M, Sýkora I, Szarka J, Pikna M, Holý K. Aerosol radioactivity monitoring in Bratislava following the Chernobyl accident. *Journal of Radioanalytical and Nuclear Chemistry*. 1988;**126**(6):467-478. DOI: 10.1007/BF02164550
- [3] Tsunami Joint Survey Group, The 2011 Tohoku Earthquake. Nationwide field survey of the 2011 off the Pacific coast of Tohoku earthquake tsunami. *Journal of Japan Society of Civil Engineers, Ser. B2 (Coastal Engineering)*. 2011;**67**(1):63-66. DOI: 10.2208/kaigan.67.63
- [4] Takemura T, Nakamura H, Takigawa M, Kondo H, Satomura T, Miyasaka T, et al. A numerical simulation of global transport of atmospheric particles emitted from the Fukushima Daiichi nuclear power plant. *Scientific Online Letters on the Atmosphere*. 2011;**7**(1):101-104. DOI: 10.2151/sola.2011-026
- [5] Hirose K. 2011 Fukushima Dai-ichi nuclear power plant accident: Summary of regional radioactive deposition monitoring results. *Journal of Environmental Radioactivity*. 2012;**111**(5):13-17. DOI: 10.1016/j.jenvrad.2011.09.003
- [6] Lai Z, Chen C, Beardsley R, Lin H. Initial spread of  $^{137}\text{Cs}$  over the shelf of Japan: A study using the high-resolution global-coastal nesting ocean model. *Biogeosciences Discussions*. 2013;**10**(2):1929-1955. DOI: 10.5194/bgd-10-1929-2013
- [7] Buesseler K, Aoyama M, Fukasawa M. Impacts of the Fukushima nuclear power plants on marine radioactivity. *Environmental Science & Technology*. 2011;**45**(23):9931-9935. DOI: 10.1021/es202816c
- [8] Behrens E, Schwarzkopf FU, Lübbecke JF, Böning CW. Model simulations on the long-term dispersal of  $^{137}\text{Cs}$  released into the Pacific Ocean off Fukushima. *Environmental Research Letters*. 2012;**7**(3):34004-34013(10). DOI: 10.1088/1748-9326/7/3/034004
- [9] Nakano M, Povinec PP. Long-term simulations of the  $^{137}\text{Cs}$  dispersion from the Fukushima accident in the world ocean. *Journal of Environmental Radioactivity*. 2012;**111**(111):109-115. DOI: 10.1016/j.jenvrad.2011.12.001
- [10] Wang H, Wang ZY, Zhu XM, Wang DK, Liu GM. Numerical study and prediction of nuclear contaminant transport from Fukushima Daiichi nuclear power plant in the North Pacific Ocean. *Chinese Science Bulletin*. 2012;**57**(26):3518-3524. DOI: 10.1007/s11434-012-5171-6
- [11] Zhao C, Qiao FL, Wang GS, Xia CS, Jung KT. 福岛核事故泄漏进入海洋的  $^{137}\text{Cs}$  对中国近海影响的模拟与预测 [Simulation and prediction of  $^{137}\text{Cs}$  from the Fukushima accident in the China seas]. *Chinese Science Bulletin*. 2014;**59**(34):3416-3423. DOI: 10.1360/N972014-00012
- [12] Rong YN, Xu R, Liang XS, Zhao YB. A study of the possible radioactive contamination in the China Seas from the Fukushima nuclear disaster. *Acta Scientiae Circumstantiae*. 2016;**36**(9):3146-3159; (in Chinese)
- [13] Rong YN, Liang XS. A study of the impact of the Fukushima nuclear leak on the East China coastal regions. *Atmosphere-Ocean*. 2018. DOI: 10.1080/07055900.2017.1421139

- [14] Shchepetkin AF, McWilliams JC. The regional oceanic modeling system (ROMS): A split-explicit, free-surface, topography-following coordinate model. *Ocean Modeling*. 2005;**9**(4): 347-404
- [15] Large WG, McWilliams JC, Doney SC. Oceanic vertical mixing: A review and a model with a nonlocal boundary layer parameterization. *Reviews of Geophysics*. 1994;**32**:363-403
- [16] Beckmann A, Haidvogel DB. Numerical simulation of flow around a tall isolated seamount. Part I: Problem formulation and model accuracy. *Journal of Physical Oceanography*. 1993;**23**:1736-1753
- [17] Mason E, Molemaker J, Shchepetkin AF, Colas F, McWilliams JC, Sangrà P. Procedures for offline grid nesting in regional ocean models. *Ocean Modelling*. 2010;**35**(1–2):1-15. DOI: 10.1016/j.ocemod.2010.05.007
- [18] Egbert GD, Bennett AF, Foreman MGG. TOPEX/Poseidon tides estimated using a global inverse model. *Journal of Geophysical Research*. 1994;**99**(C12):24821-24852. DOI: 10.1029/94JC01894
- [19] Egbert GD, Erofeeva SY. Efficient inverse modeling of barotropic ocean tides. *Journal of Atmospheric and Oceanic Technology*. 2002;**19**(2):183-204. DOI: 10.1175/1520-0426
- [20] Kawamura H, Kobayashi T, Furuno A, In T, Ishikawa Y, Nakayama Y, et al. Preliminary numerical experiments on oceanic dispersion of  $^{131}\text{I}$  and  $^{137}\text{Cs}$  discharged into the ocean because of the Fukushima Daiichi nuclear power plant disaster. *Journal of Nuclear Science and Technology*. 2011;**48**(11):1349-1356. DOI: 10.1080/18811248.2011.9711826
- [21] Bois PBD, Laguionie P, Boust D, Korsakissok I, Didier D, Fiévet B. Estimation of marine source-term following Fukushima Dai-ichi accident. *Journal of Environmental Radioactivity*. 2012;**114**(12):2-9. DOI: 10.1016/j.jenvrad.2011.11.015
- [22] Tsumune D, Tsubono T, Aoyama M, Hirose K. Distribution of oceanic  $^{137}\text{Cs}$  from the Fukushima Dai-ichi nuclear power plant simulated numerically by a regional ocean model. *Journal of Environmental Radioactivity*. 2012;**111**:100-108. DOI: 10.1016/j.jenvrad.2011.10.007
- [23] Povinec PP, Gera M, Holý K, Hirose K, Lujaniené G, Nakano M, et al. Dispersion of Fukushima radionuclides in the global atmosphere and the ocean. *Applied Radiation and Isotopes*. 2013;**81**(2):383-392. DOI: 10.1016/j.apradiso.2013.03.058
- [24] He YC, Gao YQ, Wang HJ, Ola JM, Yu L. 年日本福岛核电站泄漏在海洋中的传输 [Transport of nuclear leakage from Fukushima nuclear power plant in the North Pacific]. *Acta Oceanologica Sinica*. 2012;**34**(4):12-20
- [25] Zhao C, Qiao F, Wang G, Shu Q, Xia C. 历次核试验进入海洋的 $^{137}\text{Cs}$ 对中国近海影响的模拟研究 [Simulation of the influence of  $^{137}\text{Cs}$  from nuclear experiments on China seas]. *Acta Oceanologica Sinica*. 2015;**37**(3):15-24. DOI: 10.369/j/issn.0253-4193.2015.03.002
- [26] Aoyama M, Uematsu M, Tsumune D, Hamajima Y. Surface pathway of radioactive plume of TEPCO Fukushima npp1 released  $^{134}\text{Cs}$  and  $^{137}\text{Cs}$ . *Biogeosciences*. 2013;**10**(5):3067-3078. DOI: 10.5194/bg-10-3067-2013

- [27] Hideyuki K, Takuya K, Akiko F, Teiji I, Yoichi I, Tomoharu N, et al. Preliminary numerical experiments on oceanic dispersion of I and Cs discharged into the ocean because of the Fukushima Daiichi nuclear power plant disaster. *Journal of Nuclear Science and Technology*. 2012;**48**(11):1349-1356. DOI: 10.3327/jnst.48.1349
- [28] Liang XS, Robinson AR. Absolute and convective instabilities and their roles in the forecasting of large frontal meanderings. *Journal of Geophysical Research: Oceans*. 2013;**118**(10):5686-5702
- [29] Wu JW, Zhou KB, Dai MH. Impacts of the Fukushima nuclear accident on the China seas: Evaluation based on anthropogenic radionuclide  $^{137}\text{Cs}$ . *Chinese Science Bulletin*. 2013;**58**(4-5):552-558. DOI: 10.1007/s11434-012-5426-2
- [30] Tsumune D, Aoyama M, Hirose K. Behavior of  $^{137}\text{Cs}$  concentrations in the north pacific in an ocean general circulation model. *Journal of Geophysical Research*. 2003;**108**(108):18-11. DOI: 10.1029/2002JC001434
- [31] Liang XS. Wavelet-based multiscale window transform and energy and vorticity analysis. *Harvard Reports in Physical/Interdisciplinary Ocean Science*, Rep. No. 66. Cambridge, MA, USA: Harvard University; 2002. 411 pp